Article

Long-Term Performance Assessment of a Geosynthetic-Reinforced Railway Substructure

Ahmet F. Esen [1,2,*], Peter K. Woodward [2], Omar Laghrouche [1] and David P. Connolly [2]

1 Institute for Infrastructure and Environment, Heriot-Watt University, Edinburgh EH14 4AS, UK
2 Institute for High-Speed Rail and System Integration, University of Leeds, Leeds LS2 9JT, UK
* Correspondence: ae2023@hw.ac.uk

Abstract: Significant savings in carbon emissions, cost, and time could be achieved via the reduction in maintenance frequency, capital costs of track construction, and land used. Geosynthetic-reinforced soils offer such sustainable solutions. The experimental work presented in this paper investigates the long-term performance of a Geosynthetic-Reinforced Soil Retaining Wall (GRS-RW) system as an alternative to the conventional railway embankment. Full-scale testing was carried out on three sleeper sections of ballasted and slab tracks by simulating train loads cyclically, phased to 360 km/h. The tracks were supported by either a low-level fully confined conventional embankment or a GRS-RW substructure. The substructures were formed of a 1.2 m deep subgrade and frost protection layer, in accordance with high-speed railway design standards. The overall aim was to assess the performance of the tracks, in terms of transient displacements and total settlements. It was observed that once the GRS-RW system reached its active state, it deformed in a very similar way to a conventional embankment despite the fact that the GRS-RW system is less confined than the conventional embankment. The results indicate that the cumulative settlement of the slab track, which is due to the plastic deformation of the soil, is significantly less than that of the ballasted track, which is primarily caused by the movement of the ballast particles.

Keywords: full-scale testing; railway track settlement; geosynthetic-reinforced soil; ballasted track; slab track

1. Introduction

The sustainability of the transportation infrastructure has become a crucial issue in recent years due to the growing awareness of environmental impact. Ensuring the sustainability of railway networks is becoming an increasingly pressing issue in light of the ever-growing demand for efficient and sustainable transportation solutions. In recent years, the geosynthetic-reinforced soil (GRS) approach has emerged as a sustainable strategy.

Geogrid use has been demonstrated to be an effective reinforcing method utilised beneath ballast to prevent permanent deformation in railway tracks [1]. In addition, GRS structures have been extensively constructed along highways, especially at bridge abutments, worldwide [2–9]. For nearly 200 years, railway tracks have been supported primarily by embankments [10]. Indeed, conventional sloping embankments are still commonly used for track support over flood plains and for route and track design reasons (e.g., in China and Europe) [11]. However, in Japan, the use of geosynthetically reinforced soil substructures in conjunction with retaining walls has gained popularity as an alternative to conventional embankments, particularly for high-speed lines such as the Hokkaido Shinkansen line, a branch of the high-speed line from Tokyo [12]. In 2018, full-height rigid (FHR) facing geosynthetic-reinforced soil retaining walls were widely deployed in Japan, with a total length reaching more than 180 km [13]. Under slab and ballasted tracks, the long-term elastic and plastic behaviour of GRS structures has not been extensively examined. Particularly, the total settlement of tracks on GRS under repeated loading cycles is a subject that requires investigation.

These structures provide cost-effective solutions because they require less ground stabilisation/improvement as well as land acquisition than conventional embankments due to their reduced base area requirements (Figure 1) [14]. In addition, they offer lower residual displacements during operation, resulting in superior operational performance compared to conventional embankments. Numerous field investigations have been conducted to develop design methodologies for the materials and construction steps required to build GRS-RW structures for high-speed railways [12,13,15–22]. Overall, the retaining walls, backfill, and geosynthetics wrapped around gravel bags located directly behind the retaining walls provide structural stability. Additionally, reinforced-soil barriers tend to be more flexible than conventional retaining structures. Therefore, they can be utilised in regions where large, irregular displacements are anticipated as a result of surface movements during earthquakes.
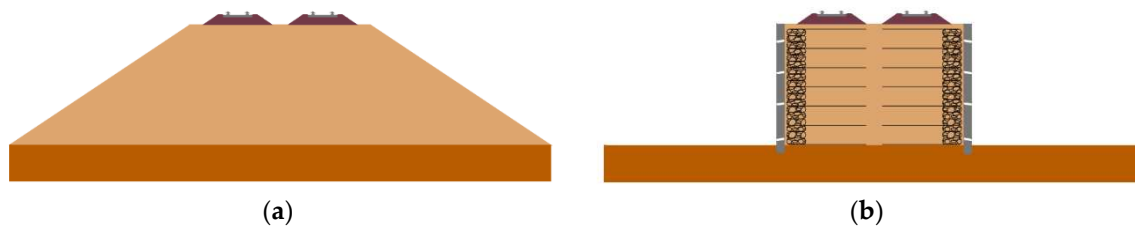

| (a) | (b) |

Figure 1. Land occupation of (**a**) a conventional embankment and (**b**) the GRS-RW system [14].

The GRS-RW system is designed with a full-height rigid facing that offers improved performance over concentrated loads, which is particularly advantageous in railway applications. Traditional reinforced wall structures that use discrete wall panels can be vulnerable to severe damage if one of the panels loses stability, posing significant concerns and issues for railways. In contrast, the GRS-RW structure utilises a minimum FHR facing concrete thickness of 30 cm, which is based on constructability considerations. This facing is thin and requires minimal steel reinforcement and exceeding the thickness requirements is solely based on structural considerations. The retaining wall has a maximum recorded height of 11 m, while the largest GRS bridge abutment is 13.4 m high [21]. It is important to note that, at low wall heights, care must be taken to prevent low confining pressure, which can cause stability issues. To address this, gravel bags are used to provide lateral support during construction.

The GRS-RW system provides many advantages over conventional cantilever structures with unreinforced soil backfill. It eliminates the need for a piled foundation to resist lateral thrust due to active earth pressure conditions, internal moments, and shear forces, particularly when constructing over soft soils and for significant wall heights. This results in a significant cost reduction and increased seismic resilience. The use of a 1 m deep cement-mixed soil with a cement content of 150 kg per cubic meter and a drainage layer consisting of crushed gravel has been implemented in an example of the GRS-RW system [19]. The compaction applied to the backfill and the induced tensile stresses in the geosynthetic reinforcement are critical elements in the construction process to reduce the lateral pressure on the facing. The use of pre-loaded and pre-stressed gravel backfill for GRS-RWs with full-height rigid facing has been successfully implemented in a railway line in Kyushu Island, Japan, and confirmed its high seismic stability capability through model shaking tests [20].

A stable GRS-RW substructure requires a strong connection between the facing and the backfill. The use of gravel-filled bags placed at the wall face provides high drainage capacity, efficiently dissipating any excess pore pressure generated in the backfill during loading. Additionally, the penetration of the facing concrete into the surface zone of the gravel-filled bags increases the contact strength between the concrete facing and the bags.

However, there are some drawbacks to the GRS-RW system. For example, the requirement of the facing to be cast in situ increases construction time and can generate issues

around the fabrication of the facing, particularly the connections of the backfill steel rods. The inability of the facing wall to support lateral loads and shear forces may be a wasted opportunity for enhancing the dynamic stability and properties of the track structure as a whole, particularly over soft soils. Improving the ground dynamic performance may help to mitigate the critical velocity effects that can occur at high train speeds.

In summary, it is clear that the cumulative settlement of the GRS-RW system requires further research work. Moreover, although Japan has utilised GRS-RW structures for railways, they required heavy reinforcement to withstand large earthquakes, which made them less cost-efficient. However, these structures proved to be resilient against ground movement. Nevertheless, the Japanese systems have not been tested for speeds exceeding 340 km/h or UK track tonnage. Therefore, it is crucial to conduct essential research to evaluate the performance of an optimised GRS-RW system with less reinforcement specifically tailored for the UK and test for speeds at 360 km/h.

This paper aims to explore the impact of geogrid use on the settlement behaviour of soil and compare the total settlement trend between the slab and ballasted tracks. To achieve this, an experimental setup of slab and ballasted tracks on a low-level confined conventional embankment and GRS-RW system is presented. It should be noted that, from now on, the conventional embankment refers to the low-level fully confined conventional embankment, for simplicity. The tests are carried out in the full-scale Geopavement and Railways Accelerated Fatigue Testing (GRAFT-II) facility. The railway track settlement mechanism and common parameters are discussed in Section 2. Details of the testing procedure and data acquisition are described in Section 3, while Section 4 discusses the results of the total settlement and elastic behaviour of the tracks. Finally, the conclusion of the study is presented in Section 4.

2. Railway Track Settlement

To understand the permanent deformation behaviour of slab and ballasted tracks on GRS-RW systems, initially, the root cause of track settlements needs to be identified. Track settlement occurs as a consequence of the plastic movement of the soil grains due to repeated loading. Soil grains, for example, will densify and hence reduce the void ratio as particles glide past each other into a new physical condition, when subjected to repeated loading. Large settlement takes place in the ballast and subgrade for new railways. For existing well-used ballasted track lines, the majority of the settlement is caused by the ballast. Even if a line has been subjected to a high level of cyclic loading and has thus developed a resilient state, fresh settlement can still occur if the train's axle load is raised. The settlement causes uneven track geometry, which requires maintenance through tamping, for example, to preserve the track level. The ride comfort for passengers would degrade if the track geometry were not rectified due to excessive oscillations in the train suspension system, known as track roughness. Further deterioration can put track stability and safety in jeopardy and could eventually lead to derailment.

The availability, maintainability, and cost of ballast make it an ideal geomaterial for railways [23]. The main functions of ballast, as stated previously [23–28] are to bear the vertical, horizontal, and longitudinal forces and to limit the movements of the particles. It helps to distribute the loads applied by trains over the subgrade and protect the subgrade from high stresses, thus, lowering permanent deformations. It also provides resiliency, absorbs vibration energy, and reduces noise. The ballast also facilitates drainage to keep water away from the track, allows maintenance, inhibits the growth of vegetation, and reduces frost problems. Despite these very important functions, as well as being cheap and practical, slab track structures are becoming increasingly used in high-speed railways to overcome the need for continuous maintenance, among other reasons. In addition to the ongoing discussion on the performance of the ballasted and ballastless (slab) tracks, alternative types of track support structures such as geosynthetically reinforced soil are also being proposed to improve the inherent track quality, while lowering the upfront capital construction costs.

Granular materials have two types of deformation under cyclic loading, resilient deformation and residual deformation. Resilient deformation is defined as the recoverable response under each cyclic load and residual deformation is the permanent deformation and is an irrecoverable strain. For either granular or cohesive soil materials, the resilient modulus *Er* (commonly referred to as *Mr*) is attained after several cycles of stress. A traditional cyclic triaxial test is usually used to gather this information (i.e., with no principal stress rotation). A hollow cylinder or real triaxial apparatus can also be used to obtain the resilient modulus. For granular soils, the resilient modulus is dependent on the confining pressure, whereas, in cohesive soils, many factors such as stress state, soil type, and physical state can influence the resilient modulus.

The fundamental equation for total settlement, i.e., the cumulative plastic deformation of soil under repeated load, was developed previously [29,30] and is given by $\mathcal{E}_N = AN^b$, where $\mathcal{E}_N$ is the plastic strain after N load cycles, and A and b are constant parameters related to the soil type, its properties, and the stress state. The constant A is replaced by $\mathcal{E}_1$, which is the plastic strain after one load cycle, in the cumulative settlement of ballast [31,32]. The equation of the plastic settlement of the ballast is highly dependent on the plastic strain of the first load increment, therefore, the initial compaction of the ballast during installation is crucial. The sub-ballast settlement equation follows the same principle used for ballast as both materials are granular. If the sub-ballast has been in place for a long time and only the ballast has been replaced during a ballast clean or renewal, the behaviour of the sub-ballast can be considered to be linear as follows $\varepsilon_N(\%) = 1.7 \times 10^{-7} \, N$ [31,32].

The coefficient A was found to vary significantly from 0.0005 to 6.3 [33]) because the soil compressive strength varies with the soil moisture and dry density. The influence of the soil's physical state is indicated by $A = a \, (\sigma_d/\sigma_s)^m$, where a and m are the material parameters, σ_d is the deviatoric stress, and σ_s is the soil static strength. The coefficient m is within the range of 1.0 to 4.2 and a is within 0.3 to 3.5 when using this method. The final cumulative settlement model developed [33] is $\mathcal{E}_p = a \, (\sigma_d/\sigma_s)^m \, N^b$ or $\mathcal{E}_p = a \, (\beta)^m \, N^b$, where $\mathcal{E}_p$ is the plastic strain and β is the stress ratio. The final subgrade settlement is calculated by adding the deformations of all n number of subdivision layers ($n = 5$ with 0.3 m thickness [33]) and applying the formula $\rho_{subgrade} = \sum_{i=1}^{n} \varepsilon_p^i h_i$, where h_i is the thickness of each subdivided layer. We must also compute the settlement in the ballast ($\rho_{ballast}$) and sub-ballast ($\rho_{sub\text{-}ballast}$) in order to calculate the track's total settlement. As a result, the total track settlement for a given number of cycles is given by $\rho_{total} = \rho_{ballast} + \rho_{sub\text{-}ballast} + \rho_{subgrade}$.

The settlement of a ballasted track is assessed considering two major phases. If a track is freshly tamped or constructed, a relatively large settlement occurs after the track is subjected to the very first loading cycles. There would not be irregularities if all points of the track settle in the same way. However, if the deformations differ along the track, track irregularities would occur [24]. The second phase of settlement is slower and tends to have a linear relationship with time/load [25]. According to the literature [24,34], dynamic loads, rail shape, and differential ballast settlement are the major causes of track deterioration. Irregularities as a consequence of differential settlement can then build up and can cause alterations in the distribution of loads [35].

Because settlement is non-linear with the number of cycles, track conditions, and different wheel loads, several versions of the cumulative settlement equation can be developed for mixed loading conditions. To understand and correctly predict the settlement behaviour of ballast, sub-ballast and subgrade, numerous laboratory and field investigations are performed to develop empirical models. A variety of previously published models on track settlement are also investigated to identify the main parameters influencing settlement. The main triggering mechanisms, as claimed previously [34], are the dynamic forces, rail shape, sleeper spacing, sleeper support, ballast settlement, and substructure. In addition to these factors, Holtzendorff and Gerstberger [36] proposed four factors which are:

1. Deviatoric Stress: the stones start moving if the deviatoric stress $\sigma_1 - \sigma_3$ exceeds the stone-to-stone friction. In this case, the horizontal stress σ_3 should be large enough to confine the ballast.

2. Vibration: when the track is dynamically loaded, the particles start spreading horizontally.
3. Degradation: due to particle friction, tamping, and various environmental effects, particle wear and breakage occur.
4. Subgrade Stiffness: the more the subgrade deforms, the more the track settles.

Dahlberg [37], Abadi et al. [38], and, Thom and Oakley [28] compared major settlement models proposed by researchers from all around the world. The most common parameters highlighted were the number of load applications (N), axle load (P), vertical pressure (σ), subgrade stiffness (k), initial settlement (S_1 and u_1), and engineering constants.

The various ballast settlement models mostly indicate similar trends. The common parameter in all settlement models is the number of cycles, where the influence depends on the relationship and whether it is linear or logarithmic. In addition, the force applied on the ballast is a significant parameter in certain equations, whereas it was not taken into consideration in others. However, the sleeper spacing, granular material type, or ballast thickness were not considered at all. The review of the settlement equations provided an overview of the settlement trends in tracks built on granular material bases.

3. Methodology

In this study, a section of a slab track and ballasted track were experimentally tested in the full-scale GRAFT-II facility under the effect of cyclic axle loading representing a moving phased loading at 360 km/h on two different substructures, namely: a low-level fully confined conventional embankment and a GRS-RW system. GRAFT-II is one of the largest railway fatigue testing facilities with a hydraulic capacity of 150 tons cyclically. It enables accelerated testing of railway tracks under realistic vertical axle loading conditions to mimic the passage of a train at a given speed.

In large experimental facilities, such as GRAFT-II, only a section of a track can be tested due to the limiting boundaries of the facility. However, the components of the tested section of the track are all in full-scale. Usually, this kind of experimental work is carried out for comparison purposes, and, in this study, the aim was to compare GRS-RW to a conventional embankment as well as a slab track against a ballasted track.

3.1. Substructures

In the scope of this research, two types of substructures are investigated. The first substructure was constructed based on conventional embankment parameters and the second substructure is the previously introduced GRS-RW system. Both structures were built using the same materials and under similar conditions, such as moisture content and compaction levels. The sand mixture was chosen from five different batches composed of 0–6 mm limestone. The sand was comprised of 80% of the 0–4 mm batch and 20% of the 2–6 mm batch. The substructure consisted of a well-graded granular limestone (according to [39]). The optimum moisture content was determined by modified proctor compaction tests, which were carried out following the procedures stated in BS 1377-4-1990 [40]. The optimum moisture content was estimated at around 4.5–5%. The effective internal friction angle ϕ' was found to be 35° at the optimum moisture content, the specific gravity parameter was 2.69, and the maximum dry density was 22.2 kN/m^3. It was expected that the moisture content would drop slightly during the testing period but would not affect the strength of the soil since the substructure was built in a controlled laboratory environment with low permeable soil. A higher optimum moisture content was identified with the standard proctor test, but the modified proctor test results were more suitable for the given substructure because a heavy compaction method was used while constructing it. A 140 kg diesel forward/reverse plate compactor with 25 kN compaction force vibrating at 90 Hz was used. The substructure consisted of two layers, namely, the subgrade and the frost protection layer (FPL). The FPL was a 40 cm layer of soil placed on top of an 80 cm deep subgrade, forming a 120 cm deep substructure. The subgrade was compacted using two passes and the FPL with four passes, with each pass consisting of forward and reverse compaction.

The TRRL DCP (Dynamic Cone Penetrometer A2465) is used to determine the structural properties of unbound materials in railway substructures and road pavements. After each compaction level, the DCP values were recorded, as seen in Figure 2a. The CBR values of the compacted soil were obtained using DCP tests. The average CBR values recorded in the GRAFT-II facility at six different locations are presented in Table 1. The same compaction method for both the conventional embankment and GRS-RW was followed. The CBR values were in good agreement, proving that the geogrid did not influence the degree of compaction. The CBR values collected from the six locations were close to each other, therefore, the mean value was considered on the spot without recording standard deviations. This indicated uniform compaction in the soil. The relationship between the DCP reading and CBR values was obtained with $\log 10(CBR) = 2.48 - 1.057 \times \log 10\left(\frac{mm}{blow}\right)$, as previously proposed [41].

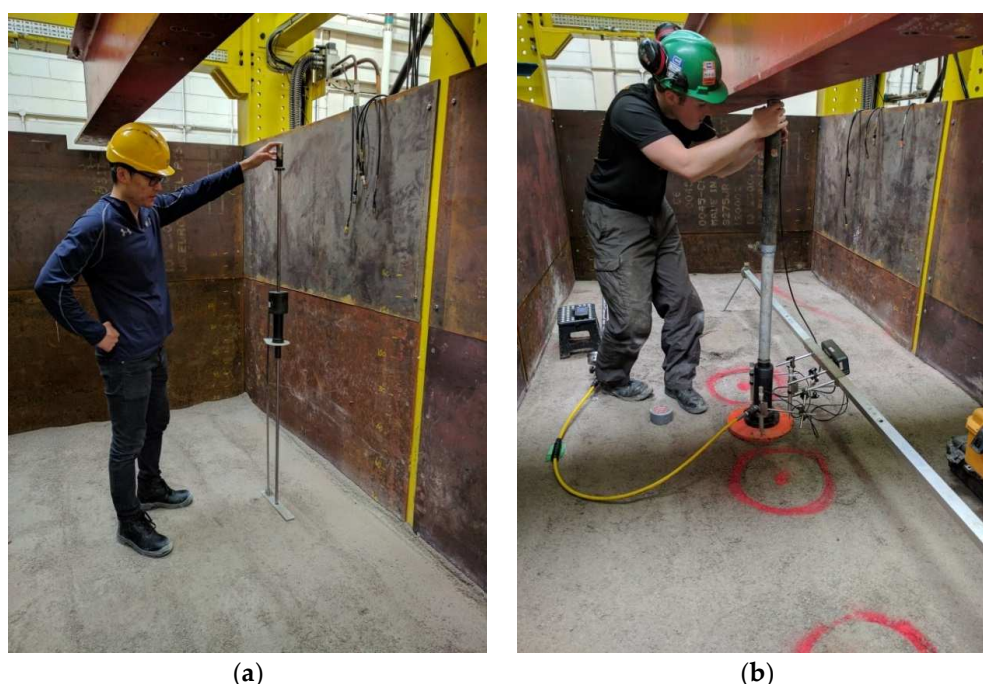(**a**) (**b**)

Figure 2. In situ soil parameter tests: (**a**) Dynamic Cone Penetrometer (DCP) and CBR investigation and (**b**) Plate Load Test (PLT) and E_{V2} investigation.

Table 1. CBR values of the compacted soil using Dynamic Cone Penetrometer (DCP).

CBR Test Time	Embankment	GRS-RW
During construction of Substructure-Subgrade	31.76	28.5
During construction of Substructure-FPL	43.36	56.1
After removal of Slab on top of FPL	120.56	125.1
After removal of Ballast on top of FPL	122.2	128.2

The elasticity of the substructure corresponded to the German ZTVE-StB 94 standard [42]. In this standard, the deflection modulus E_{V2} should be at least 120 MN/m^2 for the frost protection layer (FPL) and at least 60 MN/m^2 for the subgrade. The deflection modulus E_{V2} was verified using a static plate load test (Figure 2b) in accordance with the DIN-18134 standard [43]. E_{V1} is the static deformation modulus or the strain modulus of the first loading cycle for the bearing capacity and E_{V2} is the static deformation modulus or the strain modulus of the second loading cycle for the bearing capacity. The coefficient of permeability (k) should be between 10^{-5} m/s and 10^{-4} m/s for the FPL and the relative

density (D_r) within 98% to 100% for the FPL and subgrade density. In this work, the E_{V2} value of the FPL was estimated through the plate load test to be 133.55 MN/m^2, and E_{V2}/E_{V1} was 1.42; the permeability k was evaluated through the permeability test and was found to be 10^{-5} m/s and the D_r was 100%. Further laboratory tests revealed the E_{V2} value of the subgrade to be 67.71 MN/m^2, E_{V2}/E_{V1} = 1.55, and D_r = 98%.

The Young's modulus of the subgrade could be found using the following general equation for plate load testing; E_{PLT} = $(2P(1 - v^2))/\pi r \delta$, where E_{PLT} is Young's elastic modulus (MPa); P is the applied load (N); r is the radius of the plate (mm); v is the *Poisson*'s ratio; and δ is the plate deflection.

To build the substructure, the sand was compacted using a forward/reverse plate compactor. In order to achieve effective compaction, the sand was compacted into layers of 200 mm thickness. The compaction level was set based on a correlation between the *CBR* values, which were obtained via dynamic cone penetrometer tests, and E_{V2} values, which were obtained using the plate load tests. The correlation was derived from previous research [44] using E_{dyn} = $2E_{V2}$ = $100CBR$ [%], where E_{dyn} is the modulus of deformation at the second loading during the plate load test (MPa) and E_{V2} is the modulus at load and vibration (MPa). The right level of compaction is essential to achieve the required stiffness of the subgrade and FPL layers.

3.1.1. Conventional Embankment

Čebašek, et al., [45] provided a comprehensive description of the various stages involved in the construction of the conventional embankment. This type of embankment is referred to as "conventional" due to its adherence to the traditional standards for compaction using solely soil materials. However, it should be noted that, due to experimental testing constraints, this substructure lacked traditional slopes and was instead a fully confined, low-level embankment. The depth of the substructure, including the subgrade and FPL, was 1.2 m. A total of 52 bags of sand, each weighing 850 kg, were used to construct the substructure. The height of the subgrade was 800 mm and the thickness of FPL was 400 mm, corresponding to the German ZTVE-StB 94 standard [42]. The CBR values are presented in Table 1. Figure 3 illustrates the slab track resting on the conventional embankment.

3.1.2. GRS-RW System

The GRS-RW system was investigated in the GRAFT-II facility by Esen, et al. [14] following the same testing procedure used for a conventional embankment [45]. The substructure was made of a well-compacted base layer topped with a 1.2 m high geogrid-reinforced fill. The Tensar RE540 geogrid was used, known for its enhanced long-term tensile strength. During construction, the geogrid is placed over the base layer, and gravel bags are placed at the track ends in a brick wall pattern. The geogrid is then pulled and tightened over the bags, providing tensile strength. Pre-stressing and subsequent layers are added to reach a total height of 1.2 m. Steel tie bars are placed between the layers and connected to steel plates after the structure is formed. Self-compacting concrete fills the gap between the steel plate and the gravel bags to form a fully connected retaining wall system.

Gravel bags are crucial in the construction process to resist pressure and create a barrier between the GRS substructure and the wall. They help with compaction and drainage, making them important during construction. To achieve the required stiffness, the geogrid is cut into 11 m pieces and positioned on each 0.3 m base layer. Staggered joints are formed during construction, and three layers of sandbags are placed at 5 m intervals. Tie bars are anchored at 300 mm and 900 mm depths from the subgrade surface. The four layers of reinforced soil are constructed similarly, and the hydraulically bonded layer is placed on top of the substructure. The 80 mm gap between the GRS wall and RW is then filled with self-compacting concrete. The elasticity values are verified through DCP measurements during each layer of compaction. The CBR values are presented in Table 1. The stages of the construction of GRS-RW are presented in detail by Esen, et al. [14]. The ballasted track resting on GRS-RW is illustrated in Figure 4.
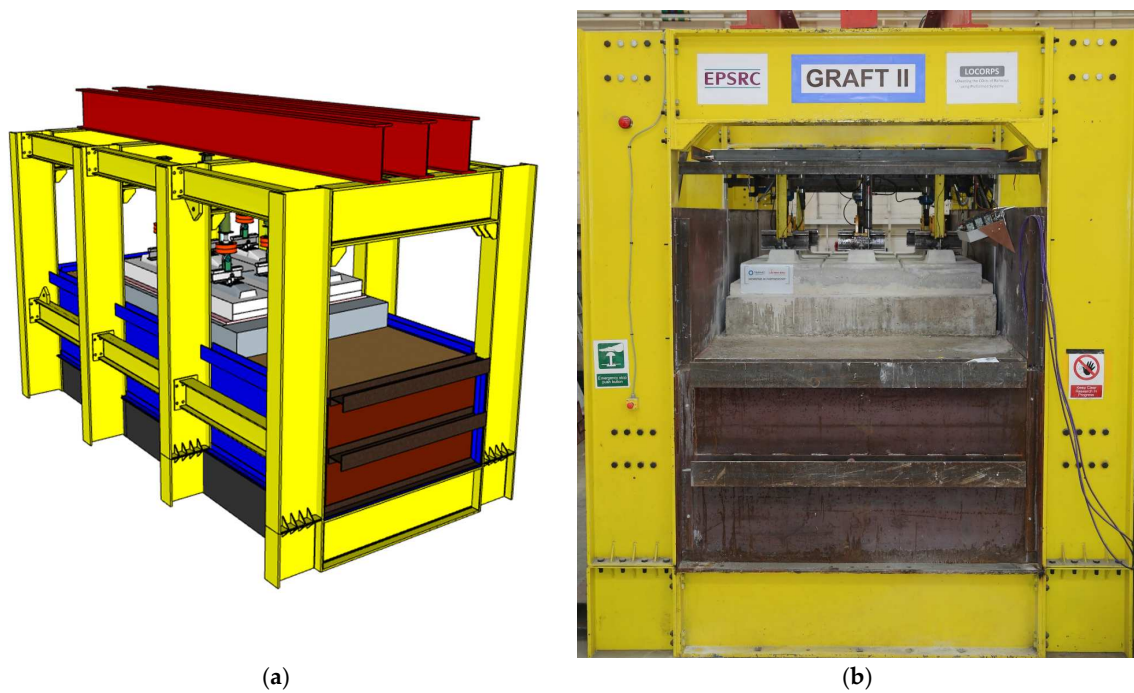
Figure 3. Slab track resting on the conventional embankment in the Geopavement and Railways Accelerated Testing Facility (GRAFT-II). (**a**) A 3D sketch of the facility and (**b**) a photo of the facility from the side view.
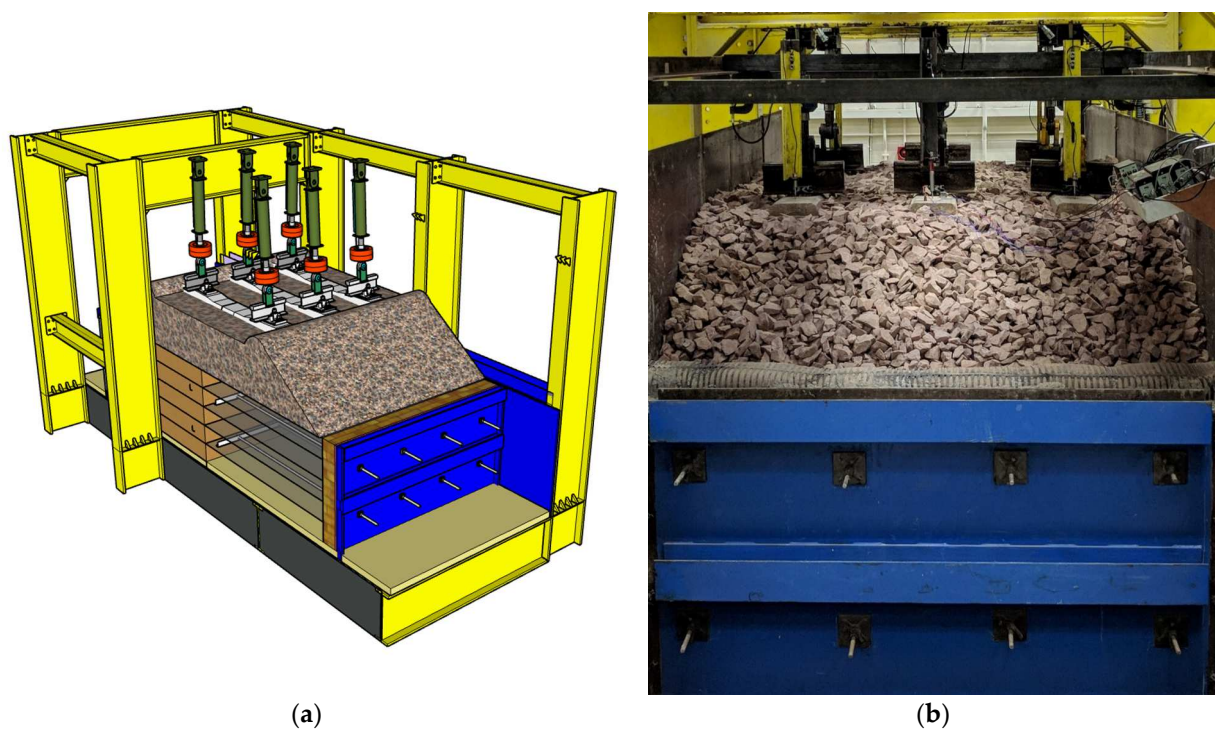

Figure 4. The layout of the ballasted track on the GRS-RW system. (**a**) A 3D sketch and (**b**) a photo of the side view.

3.2. Superstructure

Two types of superstructures were to be tested in the GRAFT-II facility, a precast concrete slab track and a ballasted track with concrete sleepers.

3.2.1. Slab Track

The first track form to be tested was a slab track. It was constructed using a Max Bögl slab track which consists of a prefabricated reinforced concrete slab made of c45/55 concrete. As shown in Figure 5, a three-sleeper section was used and placed above the Hydraulically Bonded Layer (HBL). The HBL itself was 300 mm thick and made of c10/12 concrete. After 21 days, the slab was positioned above the HBL and supported by hard wooden wedges. Then, 'Conbextra HF', a high-flow, non-shrink, cementitious grout for grouting gap thicknesses between 10 to 100 mm, was poured between the slab and the HBL.

Figure 5. Slab track in the GRAFT-II testing facility.

The chosen rail fastening system was the 300-1 Vossloh. From bottom to top, the rail support consisted of three layers: an EPDM pad, which is a soft synthetic rubber rail pad, a steel baseplate, and an EVA, which is a stiff copolymer pad for rail seating. The static stiffness of the EPDM was approximately 22.5 kN/mm and the dynamic stiffness was approximately 40 kN/mm. The static stiffness of the EVA pad was around 600–700 kN/mm and the dynamic stiffness was approximately 1600–1800 kN/mm. The cut rail segments used in the slab track test were 60E1 (UIC 60). The only purpose of the rail segments was to connect the fastenings of the slab to the actuators. The concrete slab track was subjected to more than 3 million load cycles and there was no evidence of cracks on the slab.

3.2.2. Ballasted Track

After completion of the slab track tests, the superstructure including the HBL, grout, and concrete slab, was removed from the facility. A very thin layer of the surface of the substructure soil was removed as the HBL layer had contaminated the soil particles. The upper 50 mm thickness of sand was therefore excavated and replaced with a new sand layer which was then compacted to achieve the same stiffness as the subgrade, prior to placing the ballasted track. A triangle-aperture geogrid TX190L was placed on top of the substructure to provide additional support to the ballast. This geogrid was chosen as it was the most commonly used geogrid for the traditional ballast particle size. Figure 6 shows the position of the sleepers (standard G44s) on the ballast bed at the typical spacing of 650 mm. The ballast bed was placed and compacted in four equal layers of 100 mm intervals and, hence, its overall thickness underneath the sleepers was 400 mm. In order to reach the required ballast compaction, an electric compactor with a 400 mm $\times$ 320 mm vibrating plate surface was used to compact each 100 mm ballasted layer. As a result, the bulk density of the compacted ballast was approximately 16 kN/m^3.
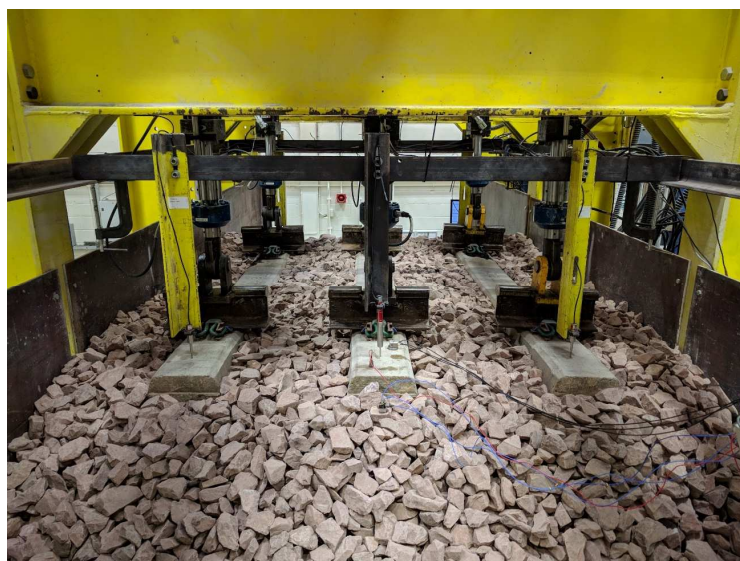
Figure 6. Ballast track in the GRAFT-II testing facility.

The lower EPDM elastic pads used in the ballasted track test were the same rail pads used in the concrete slab track test. Pandrol's fast clip fastening system was used to restrain the loaded rail segments to the sleepers. Sections of BS113A (56E1) rail segments were used in the ballasted track test. The purpose of the rail segments was to allow the connection of the actuators to the sleepers. As these were separate rail segments, they did not contribute to the bending stiffness of the track and thus they did not influence the track deformation. *It is worth noting that this is normal practice in the laboratory testing of railway tracks.* More than 3 million load cycles were also applied on the ballasted track following the same procedure applied in the concrete slab track case.

The construction process, specimen preparation, and excavation of the substructures in the GRAFT-II facility required a huge amount of team effort, lengthy tasks, and a lot of energy. Overhead cranes and forklifts were employed for handling the 850 kg sandbags, ballast, sleepers, slabs, and heavy tools. A bobcat excavator and trucks were used during the excavation process of the conventional embankment and GRS-RW. While levelling the slab was easy, thanks to the layer underneath it which was a highly fluid cementitious mixture, the sleepers in the ballast tests were hard to level due to the uneven surface of the ballast and this eventually led to some tilting during the testing. However, in the field, the continuous rails help to prevent this rotational movement, although a degree of ballast voiding may occur.

3.3. Testing Procedure and Data Acquisition

There were two static and two cyclic loading experiments conducted. During the static tests, a 13-tonne axle weight with load redistribution was applied to the track for approximately 10 min before the load was increased to simulate a 17-tonne axle load for the same amount of time. Half of the axle weight was applied to the middle sleeper (Sleeper 2), while one-fourth of the axle load was applied to each of the adjacent sleepers. (Sleepers 1 and 3). In this way, the full axle load was distributed over the three-sleeper track section during static loading. This approximation was derived from the theory of beams on elastic foundations.

After the static tests, cyclic loading began without load redistribution by applying a 13 and 17-tonne axle load on each sleeper with a time phase lag. This approach was implemented to both simulate a worst-case scenario and to allow direct comparisons of the settlement behaviour between the different track types and substructure forms for the same cyclic loading conditions. The sleepers were therefore subjected to repeated loads to simulate moving axles at 360 km/h at a set distance (frequency). The phased nature of the loading allowed for the principal stress rotation effects to be simulated. Figure 7 shows the

typical phase/time lag between the sleepers; this phasing mimics the axle moving from one sleeper to the adjacent one in 0.0065 s, which is illustrated in Figure 7. Table 2 provides the details of the static and cyclic loads.
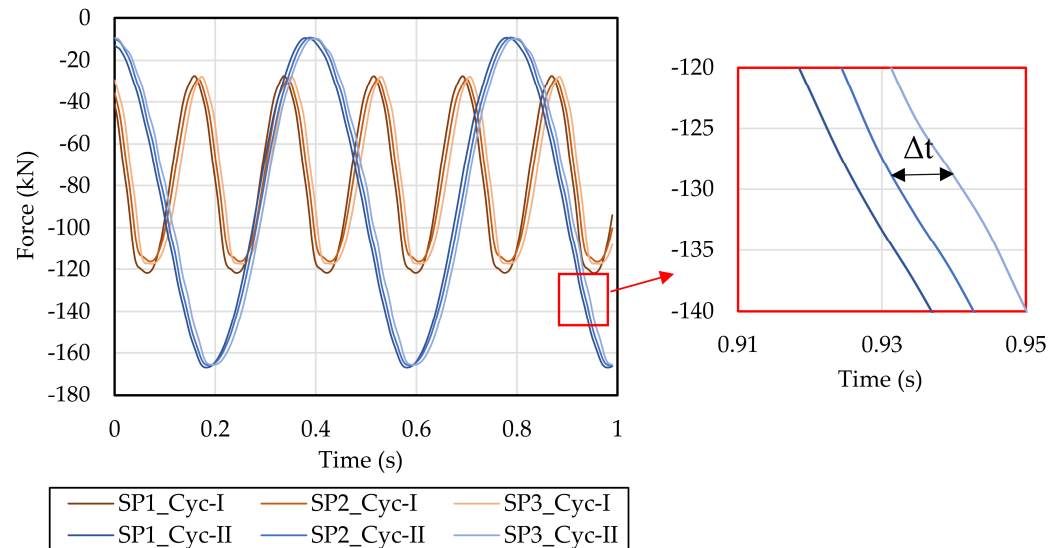

Figure 7. The time interval of the sequential actuator loading of different frequencies in a second.

Table 2. Loading sequences of the ballasted and concrete slab track tests.

Test	Static I			Static II			Cyclic I			Cyclic II		
Axle load (t)	13			17			13			17		
Duration	600 s			600 s			1.17×10^6 cycles			2.20×10^6 cycles		
Frequency (Hz)	N/A			N/A			5.6			2.5		
Δt–Time Interval (s)	N/A			N/A			0.0065			0.0065		
Load per sleeper (%)	25	50	25	25	50	25	100	100	100	100	100	100
Load per actuator (kN)	15.94	31.88	15.94	20.84	41.69	20.84	58.9	58.9	58.9	83.4	83.4	83.4
Load per sleeper (kN)	31.88	63.76	31.88	41.68	83.38	41.68	117.8	117.8	117.8	166.8	166.8	166.8

The cyclic tests were performed at two different frequencies. Initially, 1.17 million cycles (Cyclic I) were performed at 5.6 Hz and then 2.2 million cycles at 2.5 Hz (Cyclic I). The duration of Cyclic I was about 60 h without interruption, after which the testing was paused and resumed for Cyclic II, lasting for 245 h. The load applied at 5.6 Hz oscillated between 13 kN and 58.9 kN (Cyclic I) per actuator, yielding 117.8 kN per sleeper, and the load at 2.5 Hz oscillated between 5 kN and 83.4 kN (Cyclic II) per actuator, yielding 166.8 kN on each sleeper (Figure 7). The purpose behind applying 100% of the load to each sleeper was firstly to simulate the worst-case scenario, and secondly to mimic the passage of the train, which is a common type of phased cyclic load application [46].

There were 32 channels actively used to acquire data. The sampling rate of the data acquisition system was 200 Hz per channel and each item of measuring equipment was connected to a separate channel. Due to the volume of data collected, this work concentrates on those measurements from the displacement and load cell transducers only. In order to control the stroke of the actuators, six 300 mm long LVDTs were used.

Although the slab track did not consist of separate sleepers, each section of the slab was called a sleeper for comparison purposes. The LVDT choice was crucial in these tests as both deflection, which is the instantaneous/transient displacement under each cycle, and settlement, which is the irrecoverable deformation under millions of cycles, must be captured and recorded with the same LVDTs. Therefore, they needed to be sensitive enough to record the sinusoidal cyclic motion of the slab, which should acquire a hundredth of a millimetre. They also needed to be able to record the accumulated settlement of the sleepers in the ballast after 3.37 million cycles, which was greater than 10 mm. The positioning of the LVDTs on the track was, therefore, set to investigate the elastic deformation of the track as well as the total settlement under the accumulated cycles. The LVDTs were attached to an outer frame that was not in contact with the testing rig and actuators.

4. Analysis

In this section, the results related to the static and cyclic loading tests are presented and analysed. Table 3 summarises the notations and abbreviations used for the classification of the data. Different colours and shades are also used for more clarity of the figures.

Table 3. Abbreviations of the track types and sensors (Each colour represents the track type i.e., shades of yellow for ES, orange for EB, blue for GS and green for GB).

Substructure	Embankment		GRS-RW	
Superstructure	Slab	Ballasted	Slab	Ballasted
Notation	ES	EB	GS	GB
Cyclic I	CYC-I			
Cyclic II	CYC-II			
Slab/sleeper	S			
Rail	R			

4.1. Total Settlement

The cumulative settlement of the concrete slab track and ballasted track are presented in this section. The settlement data for Cyclic I and Cyclic II is analysed separately due to the variation in the loading types. Only the plastic settlement caused by the full-cyclic loading is taken into account. Cyclic I and Cyclic II represent 13 and 17 tonnes of axle load, respectively. Figure 8 shows how the data was post-processed and so indicates the computation process of plastic settlement. The figure is taken from Cyclic II loading corresponding to the ballasted track on the GRS-RW substructure as an example. The blue line indicates the force at the first actuator and the grey line represents the displacement of the rail to which the actuator was attached. As can be seen, initially, the static load increased gradually up to a certain level (point A in Figure 8); then, a low amplitude was introduced and increased until the desired magnitude was achieved (point B in Figure 8). In the case of Cyclic II, the actuators oscillated between 5 kN and 83.4 kN as can be seen in Figure 8. This adds up to a total of 10 kN and 166.8 kN load on the sleeper.

Contrary to Čebašek et al. [45] and Esen et al. [14], who included the initial settlement caused by the static loading as part of the cumulative settlement, this study focused on the plastic deformation solely caused by the load that reached full cycles (point B in Figure 8). The red dots in the figure were then obtained from 3.4 million cycles, which is a similar post-processing method used by Abadi et al. [38,47]

The average displacement values of the four LVDTs on the sleepers and the six LVDTs on the rails were then calculated. The rails and sleepers of the slab track and ballasted track, on the conventional embankment and GRS-RW substructure, were then compared for Cyclic I and Cyclic II loading.
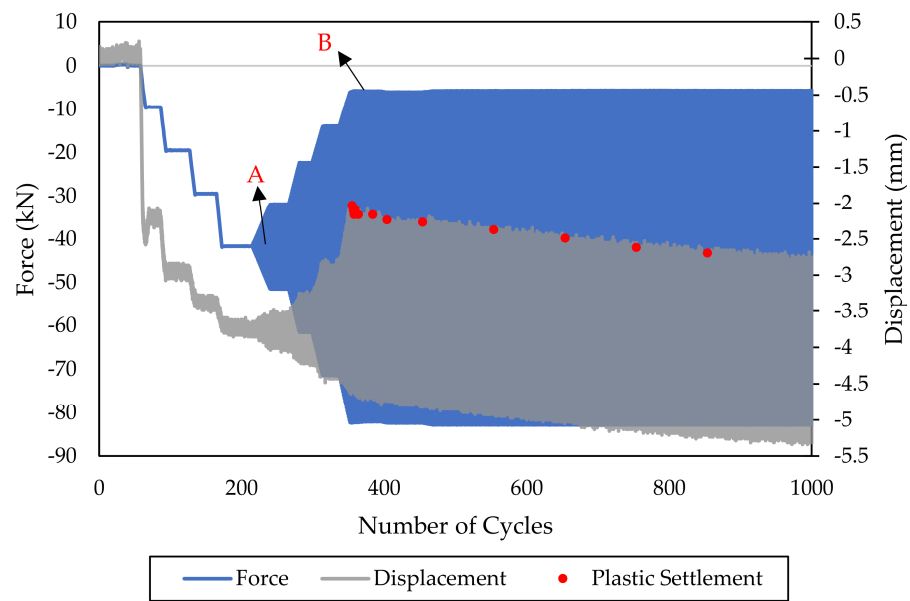
Figure 8. Plastic settlement acquisition method.

The loading cases Cyclic I and Cyclic II lasted for 1.17 million and 2.2 million cycles, respectively. Figures 9 and 10 display the total settlement of the tracks, measured by the LVDTs on the slab/sleepers, while Figures 11 and 12 show the settlements recorded based on the LVDTs on the rail. Around 40–50% of the settlement of the rails on slabs can be attributed to the plastic deformation of the rail pads. The remaining settlement results from the plastic deformation of the layers beneath the pads. The same pads were utilised for the ballasted tracks. During Cyclic I, the rail pads reached a resilient state, resulting in a nearly identical settlement between the rails and sleepers. However, in the Cyclic II tests with an increased load, the rails settled 10% more than the sleepers.
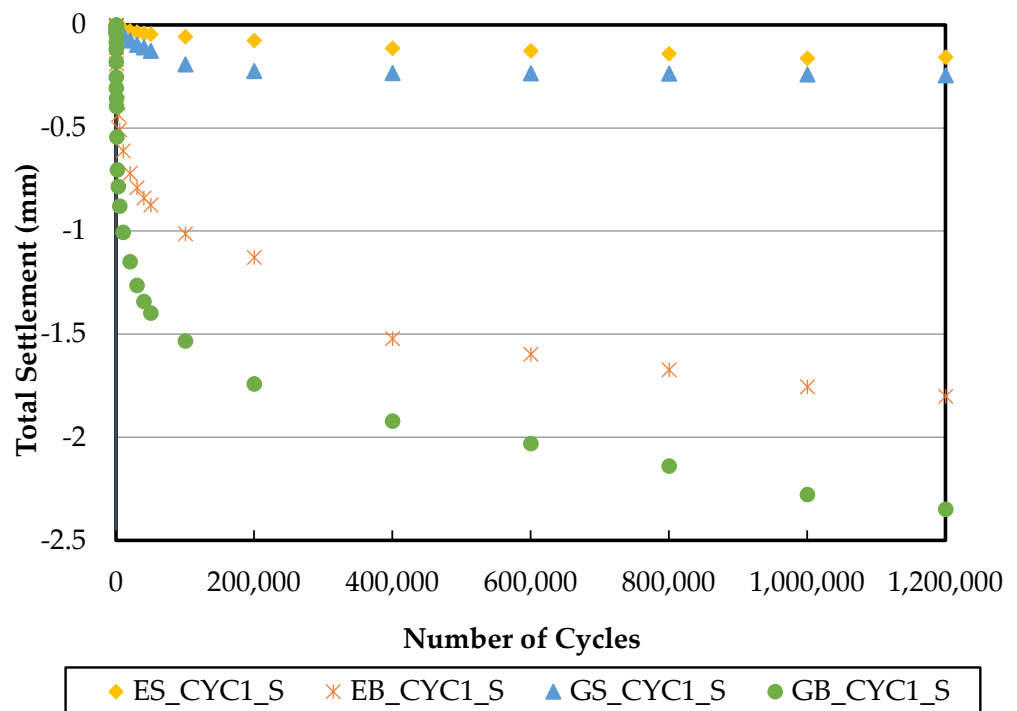
Figure 9. The total settlement of sleepers on the slab and ballasted track on the conventional embankment and GRS-RW structure for Cyclic I.
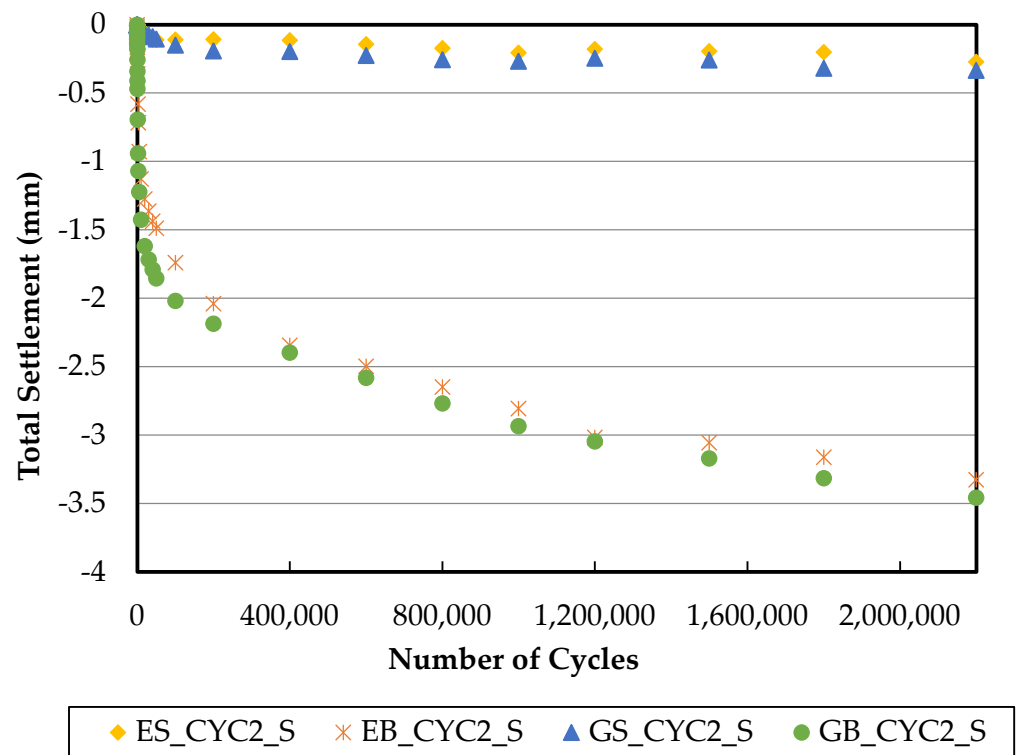
Figure 10. The total settlement of sleepers on the slab and ballasted track on the conventional embankment and GRS-RW structure for Cyclic II.
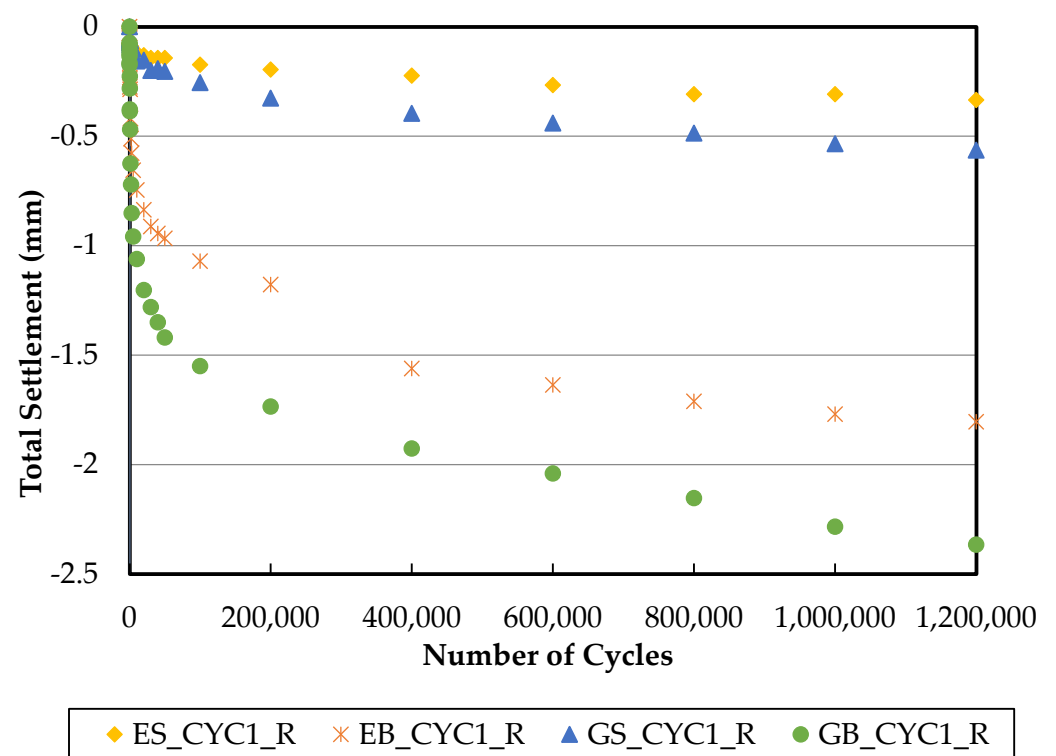
Figure 11. The total settlement of rails on the slab and ballasted track on the conventional embankment and GRS-RW structure for Cyclic I.
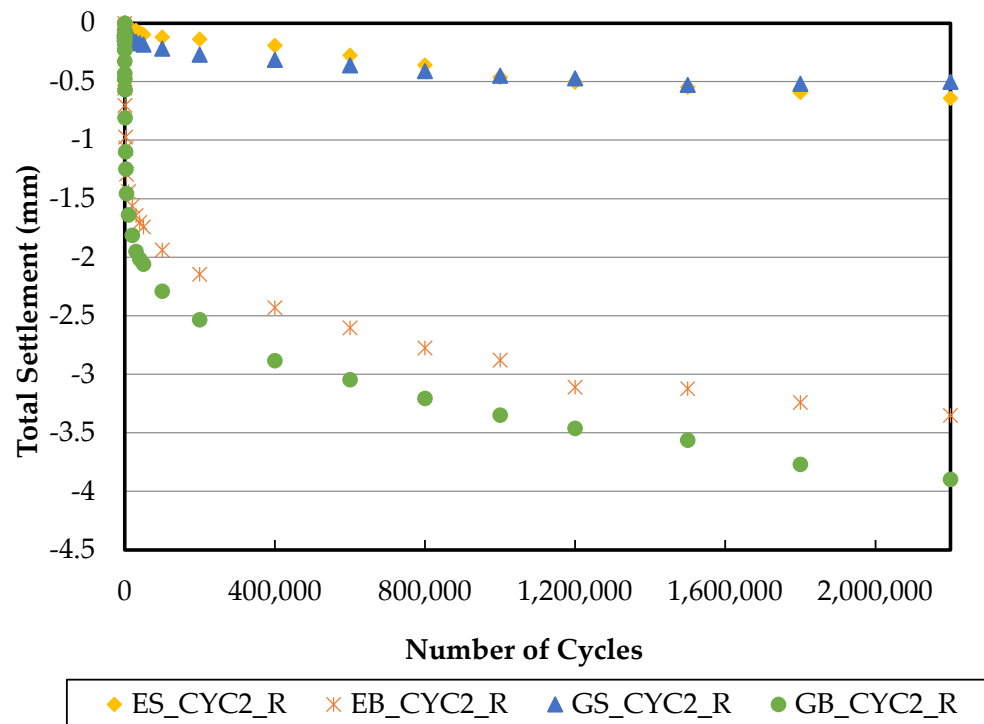
Figure 12. The total settlement of rails on the slab and ballasted track on the conventional embankment and GRS-RW structure for Cyclic II.

During the Cyclic I loading, the slab tracks settled 40% less on the conventional embankment compared to those on GRS-RW, and the ballasted tracks settled 24% less. As the GRS-RW approached a more resilient state, the slab tracks settled 28% more on the conventional embankment during Cyclic II tests. On the other hand, the ballasted track on the embankment settled only 3% less than the one on GRS-RW in Cyclic II.

The slab tracks exhibited 12 times less settlement on the conventional embankment and 10 times less on the GRS-RW compared to the ballasted tracks, indicating superior plastic deformation performance.

4.2. Analysis of Elastic Displacements and Stiffness

The rail deflections were obtained with the six LVDTs placed on the rails of sleepers 1, 2, and 3. The deflections of the sleepers of the slab and ballasted tracks were obtained using the records of the four LVDTs placed on sleepers 1 and 3, i.e., at the corners of the track. The smoothness of the cycles is directly linked to the high sampling frequency and reflects the performance of the data acquisition system. However, instead of plotting sinusoidal curves under cyclic loading, bar charts are used to represent the maximum relative displacements. The amplitudes were determined by taking 1000 cycles from the beginning of the tests and 1000 cycles before the end. The difference between the transient deflections under single cycles at the beginning and end of the loading can be then neglected since it is within the error margin of the sensors. The figures below represent the rail displacements and the average displacement values of the six rails for all four track types.

Figure 13 illustrates the displacements of the rails and sleepers under Static I and Static II loading. Sleepers 1 and 3 are indicated separately, as half of the axle load was applied on Sleeper 2 and a quarter of the load acted on Sleeper 1 and Sleeper 3. The ratio was calculated based on the displacement caused by Static II loading divided by Static I and indicated in the secondary axis of Figure 13. The force ratio, which is 17 t divided by 13 t, was 1.31. According to Hooke's law, the displacement is linearly related to the force, so the displacement ratio, mathematically, should be 1.31 too. The ratio was about 1.31 for the conventional embankment, whereas, in the GRS-RW case, the ratio was approximately 1.20 for the slab

track and 1.15 for the ballasted track. The decrease in the ratio proves that the stiffness of the GRS-RW substructure increased more sharply due to the presence of the geogrid, meaning, under certain loading, geogrids provide extra resiliency. The deformations observed in the tracks of the GRS-RW substructure under static loading were highly comparable to those of the conventional embankment. This indicates that the static stiffness of the layers under the rail of the GRS-RW substructure is similar to that of the conventional embankment, despite the fact that the conventional embankment was fully confined on all four sides while the GRS-RW was only confined on two sides. However, it must be noted that the overall stiffness of GRS-RW can still be lower than the conventional embankment.
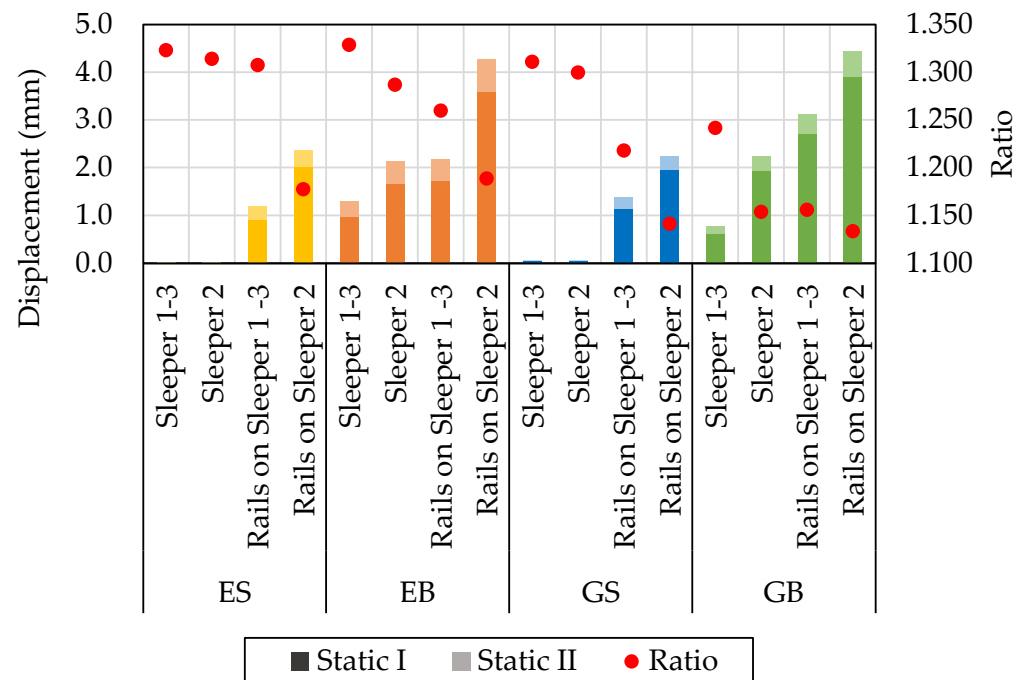
Figure 13. Average absolute displacements of the rails and sleepers under static loading (slab in the slab track case).

Figure 14 indicates the displacements of all rails and sleepers, for which the magnitude of the load on each actuator at 5.6 Hz, 'Cyclic I', oscillated between 13 kN and 58.9 kN, and for 2.5 Hz, 'Cyclic II', it oscillated between 5 kN and 83.4 kN, as illustrated by Esen, et al. [48].

The displacement of the rails on the slab was 1.14 mm and 1.21 mm on the conventional embankment and GRS-RW structure, respectively, whereas it was 1.23 mm and 1.46 mm in the case of the ballasted track. The stiffening of the tracks due to shakedown was obvious since all rail amplitudes decreased slightly at the end of the test. The reduction in the amplitude of the rail displacement was approximately 0.05 mm for all tracks.

The rails on the slab deflected in a similar way on both substructures, whereas in the ballasted track case they deflected 2.57 mm under the 83.4 kN cyclic loading, as mentioned above, which equates to a phased 17 t axle load on individual sleepers without redistribution on the GRS-RW substructure. This is 0.51 mm larger than the corresponding deflection on the conventional embankment. The reduction in amplitude in the slab rails deflection was much smaller than that on the ballasted track.

Overall, the rails deflected with the largest values on the ballasted track resting on the GRS-RW substructure (GB), as illustrated in Figure 14. On the other hand, the displacements of the rails on the slab track placed on both substructures (ES and GS) and the ballasted track on the conventional embankment (EB) were very similar, while rail deflections on ES were slightly smaller than the rest. It is worth noting that the standard deviations of the rail displacements on GRS-RW were smaller than those on the conventional embankment. The

GRS-RW substructure provided the most uniform rail deflections and, in addition to that, the slab track exhibited the lowest standard deviation. The reason for the higher deflection of the rails on ballasted track on GRS-RW could be due to the two new rail pads. The new pads may have had lower stiffness values than the other rail pads as they were not subject to any cyclic load, thus, no plastic deformation accumulated.
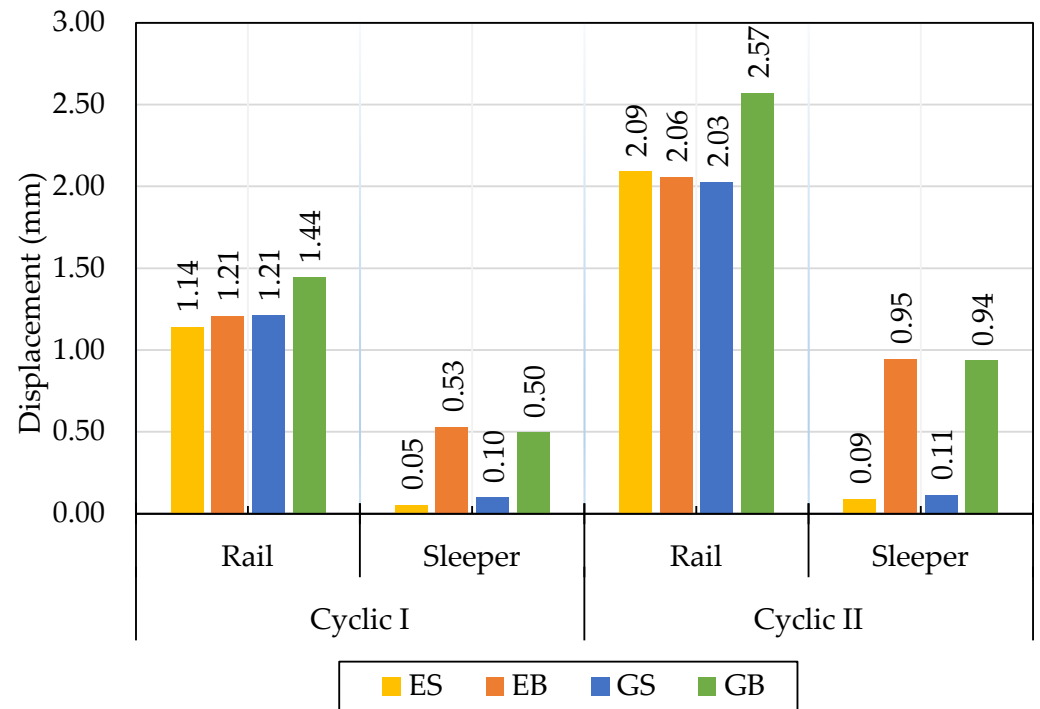

Figure 14. Average absolute displacements of the rails and sleepers under cyclic loading (slab in the slab track case), as illustrated by Esen, et al. [48].

The slab track deflected 0.05 mm and 0.1 mm on ES and GS, respectively, whereas in the ballasted track case, the deflection values were 0.53 mm and 0.5 mm on EB and GB, respectively, at 'Cyclic I'. The mean displacement of the slab under a single cycle for 'Cyclic II' loading was 0.09 mm in ES and 0.11 mm in GS. The displacements of the sleepers in the ballasted track were 0.95 mm and 0.94 mm in EB and GB, respectively.

Contrary to the elastic behaviour of the slab, the ballast reacted in a more complex manner due to its unbound nature and non-linear behaviour. While the deflection of the slab was quite uniform, according to the LVDTs on the slab, the deflection of the sleepers in the ballast varied among the LVDTs.

The stiffness of the track, including all layers under the rail, is shown in Figure 15 and the stiffness underneath the sleepers is shown in Figure 16. The reason for the significant difference in the stiffness is due to the presence of the rail pads for which the static stiffness was 22.5 kN/mm and the dynamic stiffness was 40 kN/mm. The stiffness of the pads was higher under heavier static loading, proving the pads deformed non-linearly. The stiffness of the track below the pads, on the other hand, showed similar stiffness values in both static loading cases, meaning the displacement was still behaving linearly. A 300 mm deep ballast box test was performed to identify the realistic stiffness and settlement characteristics by McDowell et al. [49] that determined the ballast stiffness as 330 kPa/mm (24.75 kN/mm), which is in good agreement with the result of the ballasted track on the embankment presented in Figure 16, as the depth of the ballast in the current test is 400 mm.
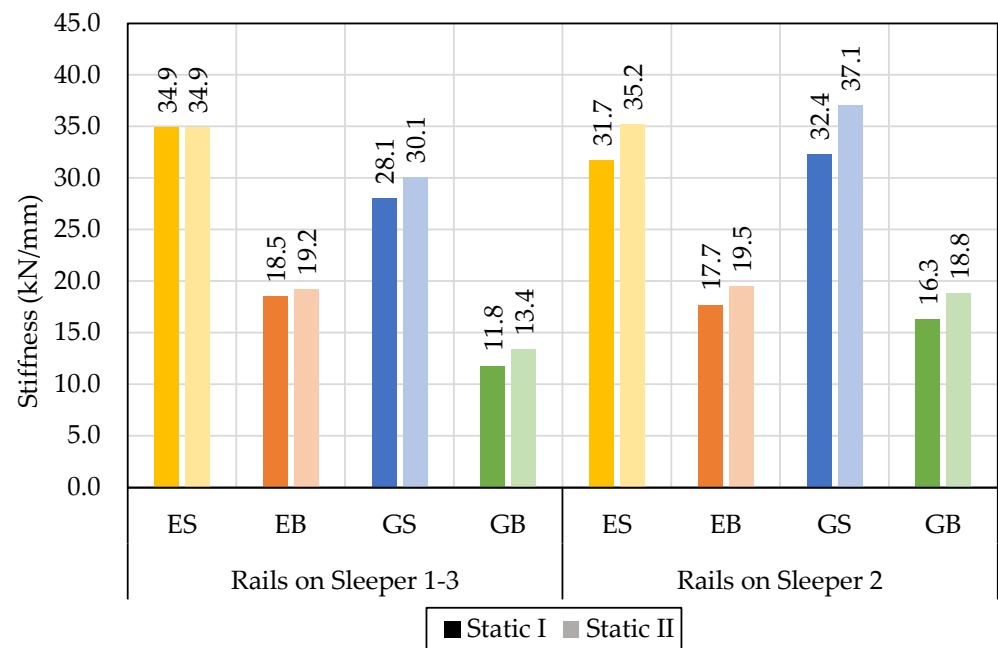
Figure 15. The stiffness of the tracks based on the deflection of the rails (including rail pads) under static loading.
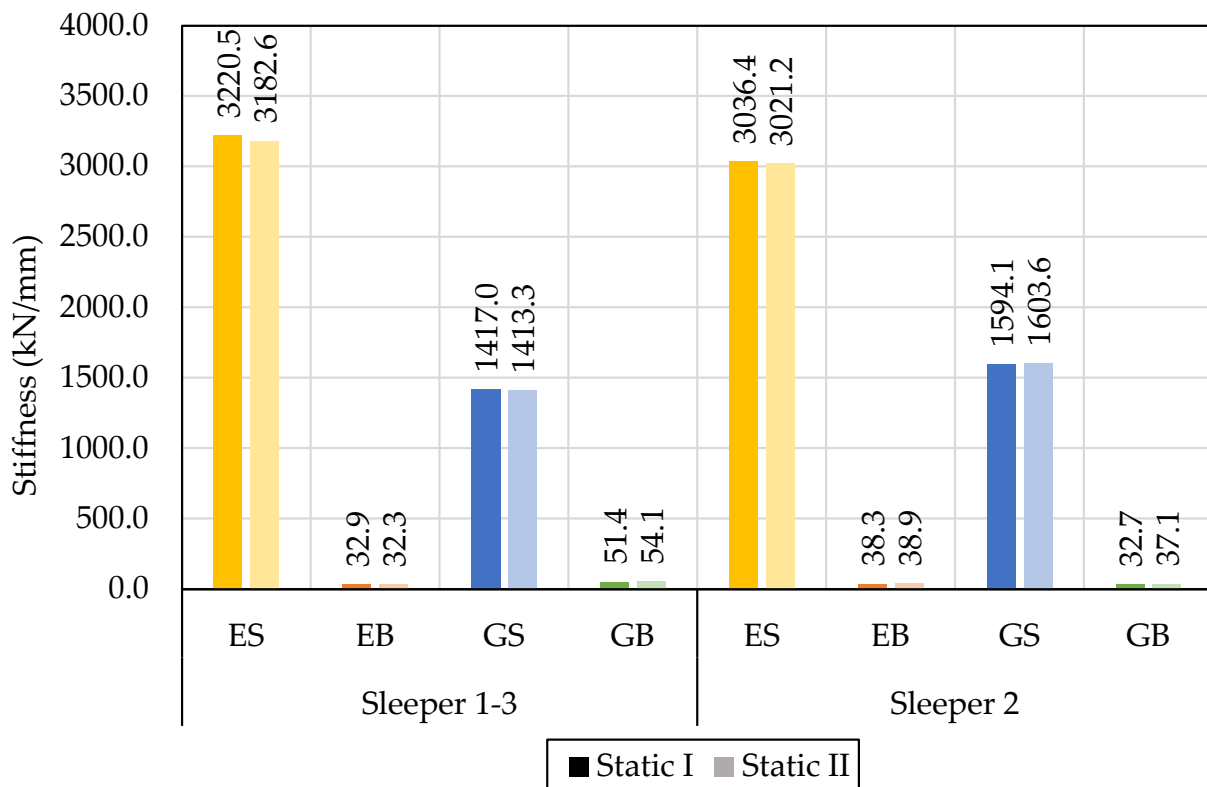

Figure 16. The stiffness of the tracks based on the deflection of the sleepers and slab (excluding rail pads) under static loading.

The stiffness levels under the rails and sleepers are shown in Figure 17. When the frequency of the loading decreased, the stiffness values also decreased despite the increase in the load magnitude at Cyclic II. The higher frequency at the Cyclic I tests dictated more of the dynamic behaviour of the soil, leading to higher stiffness levels. The soft rail pads

dominated the overall track stiffness, however, as expected, the slab track was 10 times stiffer than the ballasted track on the conventional embankment and approximately 5 times stiffer in the GRS-RW case.
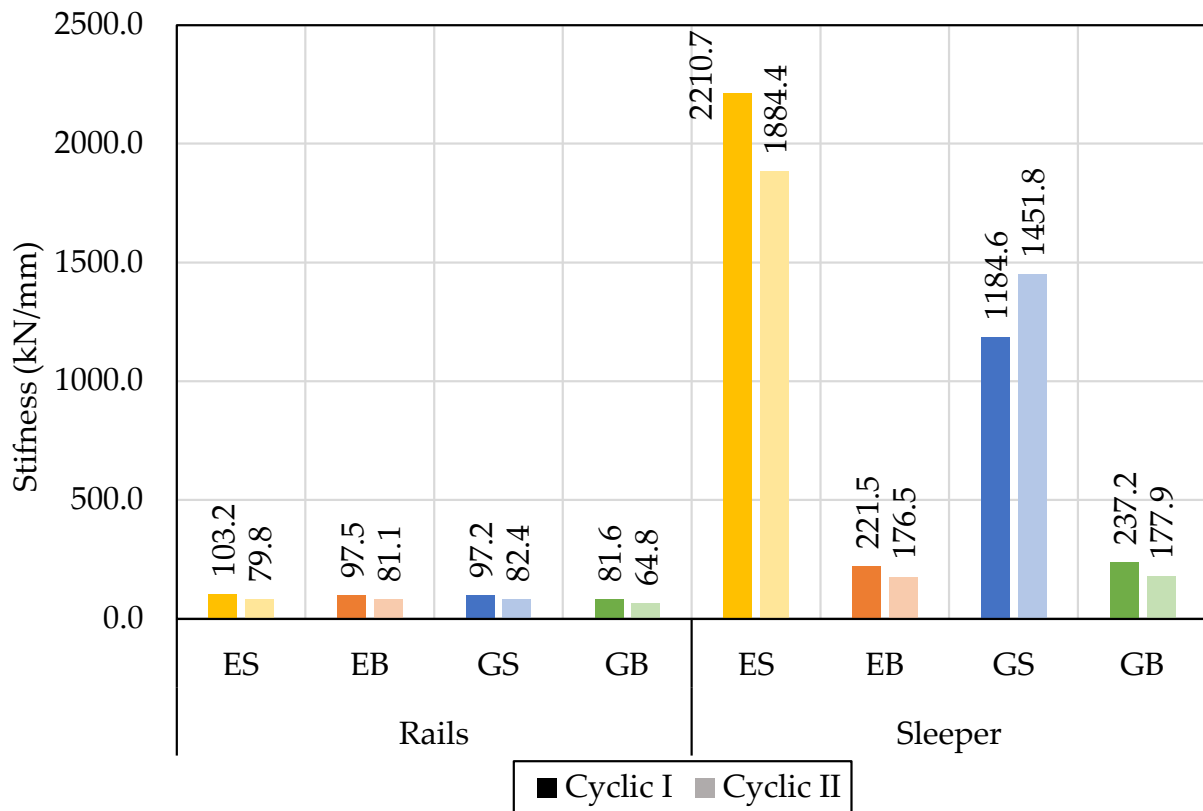

Figure 17. The stiffness of the tracks under cyclic loading.

The deflections observed in the GRS-RW were slightly higher in comparison to the low-level fully confined conventional embankment. Nevertheless, the rail deflections on all tracks imply that a train will encounter comparable displacement on both substructures. Consequently, the elastic deformation characteristics of the GRS-RW under static and cyclic loading demonstrated a striking similarity to those of the conventional embankment. It is noteworthy to mention that the conventional embankment examined in this study was fully enclosed by four walls.

4.3. Substructure Settlement Comparison

The most common parameters encountered in the settlement models, presented in Section 2, are the applied load, track stiffness, and number of cycles. As previously indicated, the deflections of the sleepers of the slab and ballasted tracks were obtained using the four LVDTs placed on sleepers 1 and 3, i.e., at the corners of the track, whereas, in the case of the rails, all six rails on sleepers 1, 2, and 3 were taken into account. Figures 18 and 19 display the overall settlement of all tracks, using the same illustration method as Abadi et al. [47] where dots are connected with lines. In the above-presented experimental results, the total settlement of the rails was higher than the settlement of the slab due to the plastic deformation which occurred in the rail pads, for the conventional embankment case, as shown in Figure 18. The plastic settlement of the rails under the same number of cycles was nearly double that of the slab. The same materials were used for the slab track and HBL in both substructures, so the smaller deformation was observed in the conventional embankment soil. The slab settlement in the case of ES at Cyclic I loading was nearly half of that of GS, whereas, during Cyclic II loading, the slab settlement was similar until about the 1,500,000th cycle. After that, the GRS-RW substructure reached

a resilient state and the settlement levelled off at 0.52 mm, while the slab track on the conventional embankment continued to settle until 0.64 mm. Another notable result is the total settlement of the slab during Cyclic I and Cyclic II. It was similar for the 1,200,000 cycles, although the load amplitude was 1.33 times greater during Cyclic II. In conclusion, the settlement of the soil under the slab tracks was dependent on the physical soil conditions and the number of cycles.
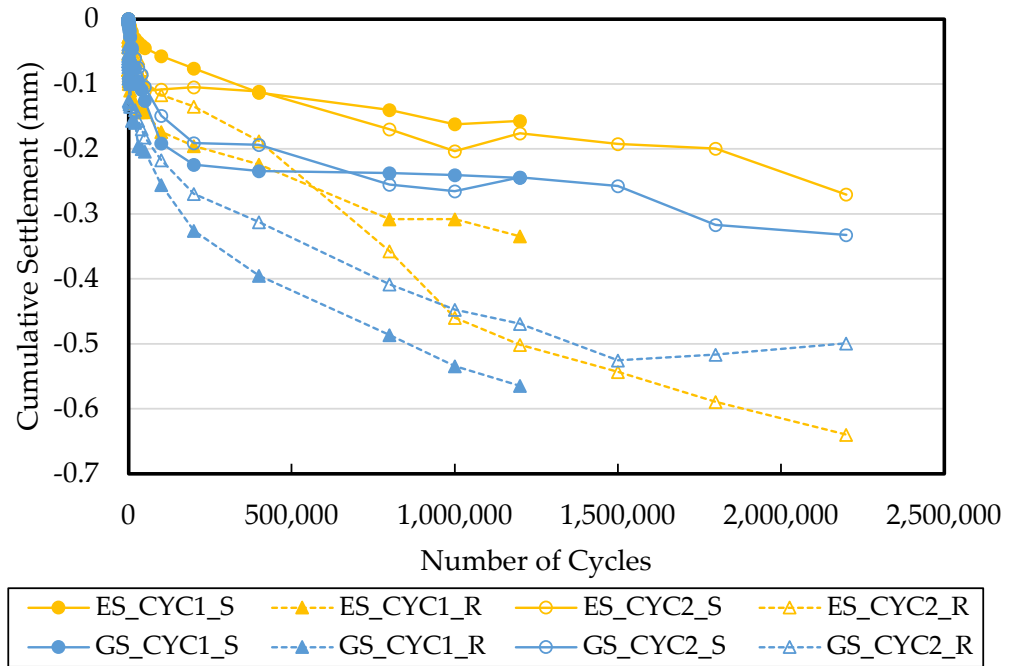

Figure 18. Cumulative settlement of rail and slab on the conventional embankment and GRS-RW structure for Cyclic I and II.
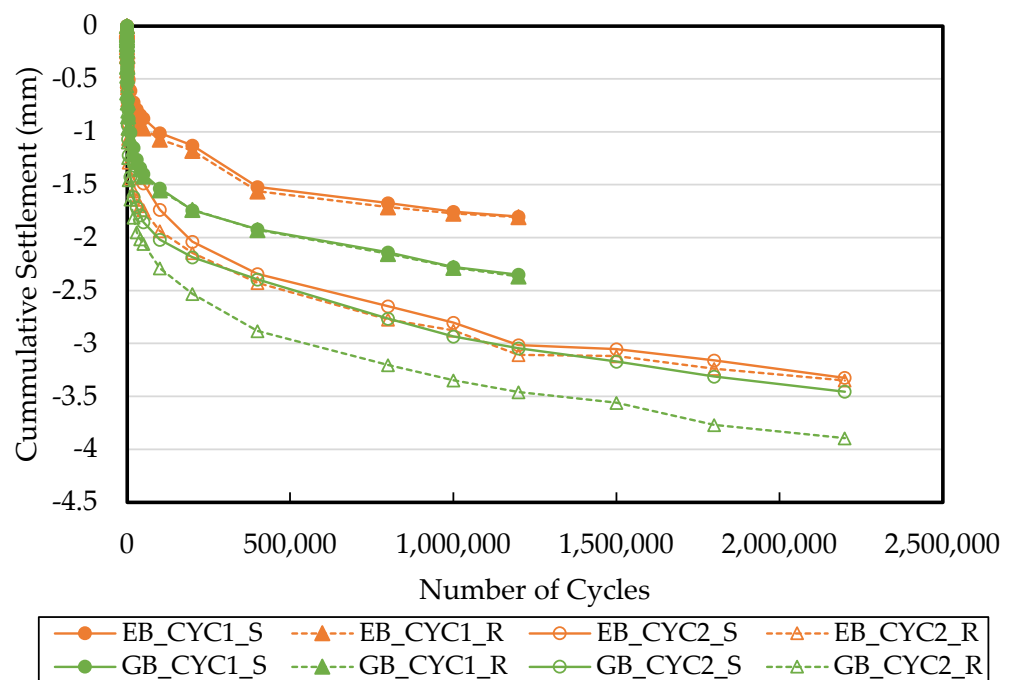
Figure 19. Cumulative settlement of the rail and sleeper on the ballasted track on the conventional embankment and GRS-RW structure for Cyclic I and II.

Figure 19 shows the cumulative settlement in the ballasted track on the conventional embankment and the GRS-RW substructure. The total rail settlement and the sleeper settlement are very similar, with less than a 1% difference, which is within the margin of the sensor error. The only exception is the initial settlement of rails during Cyclic II for the ballasted track on GRS-RW, which is higher than the sleeper's settlement. However, the trend is very similar after the initial settlement. The settlement of the ballasted track on the conventional embankment was 25% less than that of the GRS-RW substructure. The main parameters dictating the settlement of the ballasted track are the stiffness of the track, the number of cycles, and the magnitude of the axle load.

The total settlement graphs under cyclic loading showed that the difference between the rail settlement and sleeper settlement is smaller than the difference during static loading. The cumulative settlement graphs under cyclic loading included solely plastic deformation, whereas the transient displacement of rails was mainly caused by the elastic deformation of the rail pads during static loading.

5. Conclusions

In conclusion, the settlement behaviour of slab and ballasted tracks on a conventional embankment and GRS-RW substructure was examined. The experimental results confirmed the key parameters affecting the permanent settlement, as identified by settlement models found in the literature. The stiffness values based on the deflections under the static and cyclic loading cases were calculated and analysed. It was clearly observed that the concrete slab track performed significantly better, in terms of cumulative settlement and peak rail displacements, when compared to the ballasted track. The main cause for the observed higher settlement of the ballasted track was obviously due to the unbound nature of the ballast, rather than due to the settlement of the substructure, which was well compacted during the concrete slab track testing. It was even more compacted prior to the ballasted track testing as high CBR values were recorded after the slab testing was carried out. It was, therefore, concluded that had the ballasted track been tested first it would have surely experienced an even larger track settlement. Furthermore:

- The total settlement of the slab track was about 10–12 times less than that of the ballasted track. The total settlement of the slab track was caused by the plastic deformation of the soil under the HBL layer. In contrast, the settlement of the ballasted track encompassed both the ballast and the underlying soil, although approximately 95% of the settlement was attributed to the movement of ballast particles. It should be noted that the subgrade underwent significant compaction during the slab track test, thereby making ballast the primary factor contributing to the settlement in the ballasted track.
- The rails settled nearly double the slab's settlements in the slab track cases, on the conventional embankment, and GRS-RW substructure. This means the plastic deformation occurred in the pads. The rails on the ballasted track, on the other hand, settled with the same amount as the sleepers, proving the rail pads were deforming elastically under the cyclic loading.
- The settlement of the tracks on GRS-RW was nearly 20% higher than those of the tracks on the conventional embankment during the initial 20,000 cycles. Then, the settlement trend became similar for both types of substructures. It is worth noting that the slab track on GRS-RW reached a resilient state for the given loads. This was caused by the geosynthetic reinforcement in the soil. The higher initial settlement could have been caused by the consolidation of the substructure with the geogrid, which could be due to the alignment of geogrids. The geogrids start to work actively when sufficient settlement in the soil is achieved. At this stage, the GRS-RW system deforms in a very similar way to the conventional embankment despite the fact that the GRS-RW system is less confined than the conventional embankment.
- Larger total settlement values were observed in each track when subjected to lower frequency loading, primarily due to the higher magnitude of the applied load at lower

frequencies compared to higher frequencies. This finding supports the notion that cumulative settlement is influenced by the axle load as a key parameter, in addition to the number of cycles. However, it is important to acknowledge that both parameters were varied during the tests. According to the existing literature, it is generally posited that, for a given axle load, higher frequencies result in increased settlement. Both ballasted and concrete slab tracks followed typical shakedown periods even for the high formation stiffness. In the cyclic tests, a change in the amplitude of the actuator stroke after millions of loading cycles was observed. The amplitudes then slightly reduced due to the increase in the substructure stiffness, indicating plastic settlement during shakedown.

In conclusion, the experimental work presented in this paper shows that the GRS-RW system is a viable alternative to conventional railway embankments. The elastic and plastic performance of the GRS system is found to be similar to that of the conventional embankment. The performance of GRS-RW shows it is a sustainable solution with reduced land usage resulting in less environmental impact and lower maintenance intervals, hence leading to fewer carbon emissions. Thus, GRS-RW offers a promising approach to achieving an environmentally sustainable transportation infrastructure.

References

1. Yu, Z.; Woodward, P.; Laghrouche, O.; Connolly, D. True triaxial testing of geogrid for high speed railways. *Transp. Geotech.* **2019**, *20*, 100247. [CrossRef]
2. Lee, K.Z.; Wu, J.T. A synthesis of case histories on GRS bridge-supporting structures with flexible facing. *Geotext. Geomembr.* **2004**, *22*, 181–204. [CrossRef]
3. Lenart, S.; Kralj, M.; Medved, S.P.; Šuler, J. Design and construction of the first GRS integrated bridge with FHR facings in Europe. *Transp. Geotech.* **2016**, *8*, 26–34. [CrossRef]
4. Berg, R.; Christopher, B.; Samtani, N. *Design of Mechanically Stabilized Earth Walls and Reinforced Soil Slopes—Volume II*; Report No. FHWA-NHI-10-025; National Highway Institute, Federal Highway Administration: Washington, DC, USA, 2009.
5. Wu, J.T. *Geosynthetic Reinforced Soil (GRS) Walls*; John Wiley & Sons: Hoboken, NJ, USA, 2018.
6. Herold, A. *Brückenwiderlager aus KBE-Kunststoffbewehrte Erde, Einsatzgebiete und Anwendungsgrenzen*; Geotechnik-Kolloquium, Freiberg, Technische Institut für Geotechnik der Universität Bergakademie Freiberg: Heft, Germany, 2005; pp. 195–217. (In German)
7. Helwany, S.M.; Wu, J.T.; Froessl, B. GRS bridge abutments—An effective means to alleviate bridge approach settlement. *Geotext. Geomembr.* **2003**, *21*, 177–196. [CrossRef]
8. Skinner, G.D.; Rowe, R.K. Design and behaviour of a geosynthetic reinforced retaining wall and bridge abutment on a yielding foundation. *Geotext. Geomembr.* **2005**, *23*, 234–260. [CrossRef]
9. Kim, D.; Kim, U. *Performance Evaluation of a New Type of Abutment with Geosynthetics*; Civil-Comp Press: Stirlingshire, UK, 2016; p. 33.
10. Connolly, D.; Giannopoulos, A.; Forde, M. Numerical modelling of ground borne vibrations from high speed rail lines on embankments. *Soil Dyn. Earthq. Eng.* **2013**, *46*, 13–19. [CrossRef]
11. Connolly, D.; Kouroussis, G.; Woodward, P.; Costa, P.A.; Verlinden, O.; Forde, M. Field testing and analysis of high speed rail vibrations. *Soil Dyn. Earthq. Eng.* **2014**, *67*, 102–118. [CrossRef]
12. Yonezawa, T.; Yamazaki, T.; Tateyama, M.; Tatsuoka, F. Design and construction of geosynthetic-reinforced soil structures for Hokkaido high-speed train line. *Transp. Geotech.* **2014**, *1*, 3–20. [CrossRef]

13. Tatsuoka, F. Geosynthetic-reinforced soil structures for transportation: From walls to bridges. In Proceedings of the 13th Australia New Zealand Conference on Geomechanics, Perth, Australia, 1–3 April 2019.

14. Esen, A.; Woodward, P.; Laghrouche, O.; Čebašek, T.M.; Brennan, A.; Robinson, S.; Connolly, D. Full-scale laboratory testing of a geosynthetically reinforced soil railway structure. *Transp. Geotech.* **2021**, *28*, 100526. [CrossRef]

15. Horii, K.; Kishida, H.; Tateyama, M.; Tatsuoka, F. Computerized design method for geosynthetic-reinforced soil retaining walls for railway embankments. In *Recent Case Histories of Permanent Geosynthetic-Reinforced Soil Retaining Walls*; Tatsuoka, F., Leshchinsky, D., Eds.; CRC Press: Boca Raton, FL, USA, 1994; pp. 205–218.

16. Koseki, J.; Munaf, Y.; Sato, T.; Tatsuoka, F.; Tateyama, M.; Kojima, K. Shaking and Tilt Table Tests of Geosynthetic-Reinforced Soil and Conventional-Type Retaining Walls. *Geosynth. Int.* **1998**, *5*, 73–96. [CrossRef]

17. Tatsuoka, F.; Tateyama, M.; Uchimura, T.; Koseki, J. Geosynthetic-reinforced soil retaining walls as important permanent structures Geosynthetics international. *Geosynth. Int.* **1997**, *4*, 81–135. [CrossRef]

18. Koseki, J.; Bathurst, R.J.; Güler, E.; Kuwano, J.; Maugeri, M. Seismic stability of reinforced soil walls. Invited keynote paper. In Proceedings of the 8th International Conference of Geosynthetics, Yokohama, Japan, 18–22 September 2006; pp. 18–22.

19. Tatsuoka, F.; Tateyama, M.; Mohri, Y.; Matsushima, K. Remedial treatment of soil structures using geosynthetic-reinforcing technology. *Geotext. Geomembr.* **2007**, *25*, 204–220. [CrossRef]

20. Koseki, J. Use of geosynthetics to improve seismic performance of earth structures. *Geotext. Geomembr.* **2012**, *34*, 51–68. [CrossRef]

21. Tatsuoka, F.; Tateyama, M.; Koseki, J.; Yonezawa, T. Geosynthetic-Reinforced Soil Structures for Railways in Japan. *Transp. Infrastruct. Geotechnol.* **2014**, *1*, 3–53. [CrossRef]

22. Tatsuoka, F.; Watanabe, K. Chapter 23: Design, Construction, and Performance of GRS Structures for Railways in Japan. In *Ground Improvement Case Histories: Compaction, Grouting and Geosynthetics*; Elsevier: Amsterdam, The Netherlands, 2015; pp. 657–692.

23. Selig, E.T.; Waters, J.M. *Track Geotechnology and Substructure Management*; Thomas Telford: London, UK, 1994.

24. Esveld, C. *Modern Railway Track*; MRT-Productions: Zaltbommel, The Netherlands, 2001.

25. Dahlberg, T. *Railway Track Settlements—A Literature Review*; Linkoping University: Linköping, Sweden, 2004.

26. Sato, Y. Japanese Studies on Deterioration of Ballasted Track. *Veh. Syst. Dyn.* **1995**, *24*, 197–208. [CrossRef]

27. Shenton, M.J. Deformation of Railway Ballast under Repeated Loading Condition. In Proceedings of the Railroad Track Mechanics and Technology, Proceeding of a Symposium, Princeton, NJ, USA, 21–23 April 1975; Pergamon Press: New York, NY, USA, 1978; pp. 405–425.

28. Thom, N.; Oakley, J. Predicting differential settlement in a railway trackbed. In *Proceedings of the Railway Foundations Conference*; Railfound: Birmingham, UK, 2006; Volume 6, pp. 190–200.

29. Monismith, C.; Oawa, N.; Freeme, C. Permanent deformation characteristics of subgrade soils due to repeated loading. *Transp. Res. Rec.* **1975**, *537*, 1–17.

30. Knutson, R.M.; Thompson, M.R.; Mullin, T.; Tayabji, S. *Ballast and Foundation Materials Research Program. Phase IV. Materials Evaluation Study*; Champaign, III: No. FRA-ORD-77/02 Tech Report; University of Illinois: Urbana, IL, USA, 1977.

31. Li, D.; Hyslip, J.; Sussmann, T.; Chrismer, S. *Railway Geotechnics*; CRC Press: Boca Raton, FL, USA, 2015.

32. Li, D.; Selig, E.T. Cumulative Plastic Deformation for Fine-Grained Subgrade Soils. *J. Geotech. Eng.* **1996**, *122*, 1006–1013. [CrossRef]

33. Li, D.; Selig, E.T. Resilient Modulus for Fine-Grained Subgrade Soils. *J. Geotech. Eng.* **1994**, *120*, 939–957. [CrossRef]

34. Shenton, M.J. Ballast deformation and track deterioration. *Track Technol.* **1985**, 253–265. [CrossRef]

35. Iwnicki, S.; Grassie, S.; Kik, W. Track Settlement Prediction Using Computer Simulation Tools. *Veh. Syst. Dyn.* **2000**, *33*, 37–46. [CrossRef]

36. Holtzendorff, K.; Gerstberger, U. *Predicting Settlements of Ballasted Tracks Due to Voided Sleepers*; World Congress Railway Research: Cologne, Germany, 2001.

37. Dahlberg, T. Some railroad settlement models—A critical review. *Proc. Inst. Mech. Eng. Part F J. Rail Rapid Transit* **2001**, *215*, 289–300. [CrossRef]

38. Abadi, T.; Le Pen, L.; Zervos, A.; Powrie, W. A Review and Evaluation of Ballast Settlement Models using Results from the Southampton Railway Testing Facility (SRTF). *Procedia Eng.* **2016**, *143*, 999–1006. [CrossRef]

39. ASTM Committee D-18 on Soil and Rock. *Standard Test Methods for Laboratory Compaction Characteristics of Soil Using Standard Effort (12 400 Ft-lbf/ft3 (600 KN-m/m3)) 1, s.l.*; ASTM International: West Conshohocken, PA, USA, 2017.

40. *BS 1377-4-1990*; Methods of Test for Soils for Civil Engineering Purposes—Part 4: Compaction-Related Tests. British Standard Institute: London, UK, 1990.

41. *TRRL Road Note 8. A Users Manual for a Program to Analyse Dynamic Cone Penetrometer Data*; Transport and Road Research Laboratory: Crowthorne, UK, 1990.

42. Research Society of Road and Traffic. *Surface Covering Dynamic Compaction Control Methods—German Specifications and Regulations*; Additional Technical Contractual Conditions and Guidelines for Earthwork in Road Construction and Technical Testing Instructions for Soil and Rock in Road Construction; Research Society of Road and Traffic: Cologne, Germany, 1994.

43. *DIN:18134*; Determining the Deformation and Strength Characteristics of Soil by the Plate Loading Test. DIN: Berlin, Germany, 2001.

44. Lichtberger, B. *Track Compendium*; Eurailpress: Hamburg, Germany, 2005.

45. Čebašek, T.M.; Esen, A.; Woodward, P.; Laghrouche, O.; Connolly, D. Full scale laboratory testing of ballast and concrete slab tracks under phased cyclic loading. *Transp. Geotech.* **2018**, *17*, 33–40. [CrossRef]

46. Brown, S.; Brodrick, B.; Thom, N.; McDowell, G. The Nottingham railway test facility, UK. *Proc. Inst. Civ. Eng. Transp.* **2007**, *160*, 59–65. [CrossRef]
47. Abadi, T.; Le Pen, L.; Zervos, A.; Powrie, W. Effect of Sleeper Interventions on Railway Track Performance. *J. Geotech. Geoenviron. Eng.* **2019**, *145*, 04019009. [CrossRef]
48. Esen, A.; Woodward, P.; Laghrouche, O.; Connolly, D. Stress distribution in reinforced railway structures. *Transp. Geotech.* **2021**, *32*, 100699. [CrossRef]
49. McDowell, G.R.; Lim, W.L.; Collop, A.C.; Armitage, R.; Thom, N.H. Laboratory simulation of train loading and tamping on ballast. *Proc. Inst. Civ. Eng. Transp.* **2005**, *158*, 89–95. [CrossRef]